

Model based Optimal Sabatier Reactor Design for Power-to-Gas Applications

Ali El-Sibai^[a], Liisa K. Rihko Struckmann^{*[b]}, and K. Sundmacher, ^[a,b]

Abstract:

The existing infrastructure for natural gas storage and transport made the Sabatier process an attractive step within the Power-to-Gas process chain for intermittent renewable energy storage. A model-based optimal design for the methanation of carbon dioxide with hydrogen to methane under process-wide constraints is presented. After inclusion of the downstream units into the analysis, the product methane fulfils the specifications for the 'natural gas grid'. The optimization goal was to maximize the space time yield by applying the systematic flux-oriented Elementary Process Function (EPF) methodology. The optimal temperature and concentration profiles along the reaction coordinate are first determined. After that they are approximated using two reaction configurations: 1) a hydrophilic membrane reactor and 2) a cascade of polytropic reactors with interstage condensation. The results show that an optimized cascade of 3 polytropic fixed bed reactors (e.g. optimal temperature profile) and 2 intermediate condensation steps is the best technical approximation for maximizing the space time yield.

Introduction

Depletion of fossil fuel reserves, climate change, fuel prices, as well as political instabilities have recently speeded up the development of technologies that exploit renewable sources to meet future energy demands in a sustainable way. Electrical power generated from renewable sources like wind and solar can reduce our dependence on fossil fuels. However, the intermittent nature of renewable electricity perturbs the operability of the electrical grid. Therefore, a renewables-derived energy system requires energy storage as one essential system component. The 'Power-to-Chemicals' concept responds to this need by converting renewable electrical power into chemical energy carriers. The already existing infrastructure for natural gas storage, transport and utilization makes the Sabatier

process a preferential route within the 'Power-to-Chemicals' alternatives. Having a reported efficiency of 80%^[1], the route utilizes CO₂ from biogas or power plants to convert renewable H₂ into synthetic natural gas (SNG) according to Equation (1):



The recycling of the CO₂ which contributes to global warming, is another benefit from the Sabatier process.

Several processes were developed in the 70's, amid the fuel crisis, to convert syngas derived from coal and biomass gasification into SNG.^[2] However, the technology development ceased in the mid 80's following the drop in oil prices.^[2a] The methanation reaction remained, nevertheless, a purification step for hydrogen-rich streams in refineries and in chemical processes e.g. ammonia synthesis.

The renewed interest in CO₂ methanation as a 'power-to-gas' technology is reflected in the numerous recent publications exceeding 100 papers in 2014.^[3] The research focused mostly on the preparation of highly stable and active catalysts and to some extent on the elucidation of the reaction mechanism and the process/reactor design as reported in comprehensive reviews.^[3-4]

CO_x methanation is usually carried out in fixed bed reactors.^[4a] In ammonia synthesis the reactors are typically operated adiabatically, which is possible due to the low concentration of carbon oxides.^[5] However, in case of CO_x-rich feed, intermediate cooling has to be integrated with the adiabatic reactors if high CO_x conversion is desired. Indeed, a series of adiabatic fixed bed reactors with intermediate cooling and/or product recycling, as well as isothermal fluidized bed reactors were the main reactor configurations applied in the former 'coal/biomass to SNG' processes.^[2a] The adiabatic reactor/intercoolers concept was recently proposed by several researchers for the "Power-to-SNG" approach. De Saint Jean *et al.*^[6] presented a process design that consisted of a high temperature steam electrolyser, a methanation unit and a gas purification. The methanation unit consisted of a series of four adiabatic reactors with intermediate cooling and one condensation step. Shaaf *et al.*^[7] analyzed two concepts where the first consisted of two reactors with intermediate condensation and the second included six reaction stages with four gas intercooling steps.

Apart from using adiabatic reactors, the Sabatier process can be intensified by tailoring the temperature profile inside the reactor. El Sibai *et al.*^[8] reported that a combination of an adiabatic reactor with active co-current and counter current cooling is the cost optimal reaction route in a cascade with three multi-tubular

[a] Ali El-Sibai, Prof. K. Sundmacher
Process Systems Engineering
Otto-von-Guericke University Magdeburg, Universitätsplatz 2,
D-39106 Magdeburg, Germany

[b] Dr. L. K. Rihko-Struckmann*, Prof. K. Sundmacher
Process Systems Engineering
Max Planck Institute for Dynamics of Complex Technical Systems
Sandtorstr. 1, D-39106 Magdeburg, Germany
E-mail: rihko@mpi-magdeburg.mpg

reactors and two intermediate condensation steps. The company SolarFuel proposed a cascade of two polytropic tube bundle reactors with intermediate condensation.^[1] Kievidt and Thöming showed that the methane yield was improved by two folds compared to the adiabatic and isothermal operation when the reactor axial temperature profile was optimised by the Semenov number optimisation method.^[9]

Three phase reactors have also been considered for CO₂ methanation due to their good heat dissipation and tolerance to rapid load change.^[10] However, the effective reaction rate in the multiphase reactors is limited by slow mass transfer at the liquid side.^[10] Götz *et al.*^[11] proposed a reactor concept consisting of two serial reactors: an isothermal slurry bubble reactor and a polytropic honeycomb reactor with one intermediate condensation step. Full conversion could be achieved with a methane content higher than 95%.

A membrane fixed bed reactor was experimentally investigated by Ohya *et al.*^[12] They reported an 18% higher conversion with the membrane application compared to that of a typical fixed bed. However, the main drawback of the membrane was limited permselectivity for steam since all the components permeated and H₂ showed the highest permeable flux.

Holladay *et al.*^[13] and Brooks *et al.*^[14] developed microchannel methanators for in-situ propellant production systems for challenging space missions.

Nevertheless, to the best of our knowledge, no methodical study has been performed to optimally design and operate the reaction section of the Sabatier process under process wide constraints (e.g. NG grid quality specifications, feed composition/flow rate). Therefore, in this contribution, enhancement measures to maximize the space time yield (STY, [mol s⁻¹ m⁻³]) were systematically investigated by applying the Elementary Process Function (EPF) design methodology.^[15] STY was maximized by optimizing the temperature profiles, defining optimal inlet conditions and geometric dimensions of the reactors, and analyzing different strategies for the extraction of product water. The performance of a multitubular reactor cascades with intermediate condensation steps was compared to that of multitubular reactor integrated with a highly permselective hydrophilic membrane. The reactors were designed using a recently published kinetic model for the Sabatier reaction utilizing a highly active and selective Ni-based catalyst.^[16]

Previously, the EPF design methodology was used in designing optimal reactors and processes for gas-solid and gas-liquid heterogeneous reactions, e.g. for ethylene oxide production.^[17] The present study demonstrates the applicability of the methodology to a topic relevant to renewable energy conversion.

2 Optimal Reactor Design

Due to the strict specifications of water content for the methane to be fed-in into the natural gas grid, the reaction section for CO₂ methanation is integrated with a downstream drying step (e.g. glycol unit, see Fig. 1).

The reactor for CO₂ methanation is systematically analyzed and optimized in the following chapters. According to the EPF methodology, three design levels with increasing modeling complexity are defined and the corresponding decision structure is illustrated in Fig. 2.

2.1 Level 1

In Level 1, the reactor is represented by a fluid element that is freely influenced by external heat and component fluxes ($q_{ex}(t)$, $j_i(t)$) and by an internal reaction flux ($r_{rxn}(t)$) along the reaction coordinate. These fluxes act as decision variables that guarantee optimal distributed profiles of the state variables (e.g. $T(t)$, $x_i(t)$, $p(t)$) i.e. optimal reaction route. Depending on the fluxes allowed, different cases are investigated in this level, e.g. in Case 1 only heat flux $q_{ex}(t)$ is allowed, (see Table 2).

Since the aim in Level 1 is to unveil and compare quantitatively the **potential** of the different integration concepts (Cases in Table 2), no technical or transport kinetic limitations are enforced on the external fluxes. In other words, $q_{ex}(t)$ and $j_i(t)$ can be varied such that any optimal temperature and component concentration profiles are allowed.

The internal flux ($r(t)$) – rate of reaction - is defined by the type of catalyst used. Several noble and transition metals (e.g. Ni, Ru, Rh, and Co) on various oxide supports (e.g. TiO₂, SiO₂, MgO, and Al₂O₃) have showed high activity to catalyze the methanation reaction.^[18] The most active and selective (100% selectivity) are the Ru-based catalysts.^[18] However, due to the high cost of the noble metals, their use is preferred only in special applications where very compact reactors are required (e.g. space applications). For industrial SNG processes, e.g. for CO₂ methanation as discussed here, nickel based catalysts are relatively inexpensive and highly active, and are therefore considered in this study.

An intrinsic kinetic model for CO₂ methanation over Ni/Al₂O₃ was

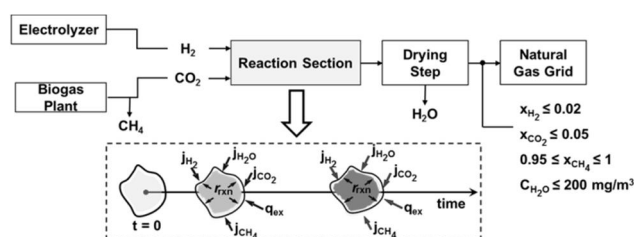


Figure 1. The general scheme of the Sabatier process. The reaction step depicted according to the EPF approach by the fluid element and integrated with a downstream drying process.

recently published by Koschcany *et al.*^[16] The model is based on the Langmuir-Hinshelwood mechanism, and is very suitable for this study since the kinetic experiments were performed under process relevant conditions:

$$453 \leq T \leq 613 \text{ K}$$

$$1 \leq p \leq 15 \text{ bar}$$

The detailed rate equation and the used parameter values are given in the Supplementary material of this paper.

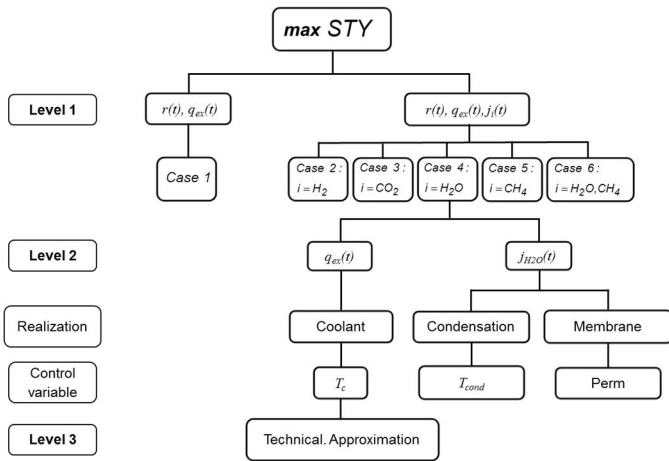


Figure 2. The decision structure of the reaction section design based on the EPF methodology

2.1.1 Model Formulation

The fluid element is infinitely small and is assumed to be ideally mixed. It is described using a pseudo-homogeneous model consisting of component mass and energy balance equations in Lagrangian formulation.

The fluid element is assumed to be randomly packed with spherical catalyst particles with a void fraction $\epsilon=0.38$.

The component mass balance is defined as

$$\frac{dn_i}{dt} = J_i r_{rxn} r_c \frac{(1-\epsilon)}{\epsilon} V_g + a_i j_i \quad (2)$$

where $a_i = \begin{cases} 1 & \text{for dosing of component } i \\ 0 & \text{no dosing/removal of component } i \\ -1 & \text{for removal of component } i \end{cases}$

In this example, we assume that the CO_2 originates from the effluent of an average sized biogas plant ($1100 \text{ Nm}^3 \text{ hr}^{-1}$, see Table 1). The CO_2 stream is assumed to be CH_4 free as obtained after CO_2 separation in the biogas plant. The ratio of H_2 to CO_2 , inlet temperature, and inlet pressure are all decision variables.

Table 1. Composition of the biogas

Component	CH_4	CO_2	O_2	H_2O
Mole fraction	0.64	0.325	0.01	0.025

The quality of the produced SNG is specified such that it can be injected directly into the natural gas grid or used as fuel for cars in Germany (DVGW G260/A, 2013 and DIN 51624):

$$\begin{aligned} 0 &\leq x_{\text{H}_2, \text{out}} \leq 0.02 \\ 0 &\leq x_{\text{CO}_2, \text{out}} \leq 0.05 \\ 0.95 &\leq x_{\text{CH}_4, \text{out}} \leq 1 \\ 0 &\leq C_{\text{H}_2\text{O}, \text{out}} \leq 200 \text{ mgm}^{-3} \end{aligned}$$

The energy balance is formulated in terms of temperature. It is assumed that the enthalpy change due to extraction/dosing of

compounds and pressure changes is negligible compared to the heat released by the reaction or the heat exchanged for cooling/heating, q_{ex} . This is a reasonable assumption considering the high exothermicity of the methanation reaction. Since q_{ex} is assumed to be unlimited in Level 1, the temperature of the reaction mixture can vary freely within the applicability of the kinetic equations: $453 \leq T \leq 613 \text{ K}$. The optimal temperature profile over the reaction time is expressed as Equation S5 in the Supplementary material. The rigorous modeling of the drying unit exceeds the scope of this work and is therefore modeled here as a black box using a simple mass balance.

The optimal reaction route (e.g. optimal profiles for T and x_i) is calculated for the Cases 1 to 6 (Table 2) by solving the dynamic optimization problem. The optimization problem is constrained by ordinary differential equations (balances), algebraic equalities and inequalities, as well as inlet and outlet conditions. The optimization problem is converted to a nonlinear programming (NLP) using orthogonal collocation on finite elements and is solved using an appropriate NLP solver (CONOPT).

The objective function for Level 1 is defined as:

$$STY = \frac{n_{\text{CH}_4, \text{prod}}}{\int_0^t \frac{V_g}{e} dt} \quad (3)$$

Mathematically, the dynamic optimization problem is defined as:

$$\max_{q_{ex}(t), j_i(t)} STY$$

s.t:

- Component mass and energy balance equations (Eqs. 2 and S5)
- Chemical reaction kinetics (Eqs. S1 to S4)
- Intrinsic bounds e.g. temperature, pressure.
- State equations e.g. Ideal gas law
- Mass balance of the downstream dehydration process

2.1.2 Result and Discussion for Level 1

Depending on the fluxes which are selected as decision variables in Cases 1 to 6, different optimal reaction routes (e.g. optimal profiles for T and x_i) are determined. The resulting STY for each case is summarized in Table 2:

Table 2. Level 1. Allowed heat and component fluxes in Cases 1 to 6 and the optimised space time yields.

Decision variables	Case 1	Case 2	Case 3	Case 4	Case 5	Case 6
$q(t)$	X	X	X	X	X	X
$j_{\text{H}_2}(t)$		X				
$j_{\text{CO}_2}(t)$			X			
$j_{\text{CH}_4}(t)$					X	X
$j_{\text{H}_2\text{O}}(t)$				X		X
STY [$\text{molm}^{-3} \text{ s}^{-1}$]	15	15	15	997	51	1143

The optimization results of Level 1 show that dosing of H₂ or CO₂ over the reaction time is not favored: $j_{H_2}(t)=0$ and $j_{CO_2}(t)=0$ in Cases 2 and 3 respectively. The STY of these two cases (STY=15 molm⁻³s⁻¹, see Table 2) is equal to that of Case 1 where only cooling ($q_{ex}(t)$) is enforced to obtain the optimal T profiles (Figure 3a). In Cases 1 to 3, the highest allowed temperature 613 K should initially be applied up to a conversion level of 0.957. Due to thermodynamic limitations, optimally a gradual reduction of the reactor temperature from 613 K to 492.7 K should then follow, to achieve finally a conversion level of ≈ 0.995 . This conversion level is required in order to fulfill the natural gas grid specifications after the downstream drying step.

By extracting the products H₂O (Case 4), CH₄ (Case 5) or both (Case 6), the equilibrium shifts towards the product side according to the Le Chatelier principle. Thermodynamic limitation is overcome and the optimal temperature is always at the upper bound (613 K) for maximum enhancement of the reaction rate (see Figure 3a). The level of enhancement, nevertheless, is dependent on the components extracted. Figure 3b shows the conversion as a function of dimensionless reaction time (normalized to the reaction time of Case 1) for the Cases 1, 4, and 5. The desired conversion ($X \approx 0.995$) is achieved in much shorter time when H₂O or CH₄ is extracted: 1.5% and 36% of total reaction time of Case 1 respectively. In all cases, the conversion increased initially very fast. However, after a conversion of 0.95, the rate decreases significantly for Case 1 and 5. The decrease is more pronounced in Case 1 due to the thermodynamic limitations. More than 60% of the reaction time is due to increase the conversion from $X=0.95$ to 0.995.

The STY values of the different cases clearly show that water removal (STY=997 molm⁻³s⁻¹, Case 4) is more beneficial than extracting methane (STY=51 molm⁻³s⁻¹). Nevertheless, the calculated space time yield in Case 6 where both products are simultaneously extracted was as high as 1143 molm⁻³s⁻¹. This is only 15% higher than Case 4. Since no simple technology for the extraction of CH₄ from a H₂ and CO₂ mixture exists, cooling coupled with water removal (Case 4, e.g. condensation or membrane) is considered to be the most promising integration concept.

Figure 3c shows the optimal profile of j_{H_2O} and the component mole fractions as a function of reaction time for Case 4. Water is continuously removed to keep the water content minimal over the entire reaction time. Initially, j_{H_2O} is at approximately 125 molm⁻³s⁻¹ and then it gradually decreases close to zero along the reaction time, as the reaction rate decreases.

In the next stage, Level 2, solutions for technically realizing the optimal profiles of j_{H_2O} and q_{ex} , obtained in Level 1 for Case 4 are analyzed in detail.

2.2 Level 2

Case 4, which is the most promising in Level 1, is investigated in Level 2. Mechanisms for attaining the desired profiles of j_{H_2O} and q_{ex} are elaborated here.

For the removal of H₂O, two alternatives are compared. Firstly, cascades of polytropic reactors with interstage condensation

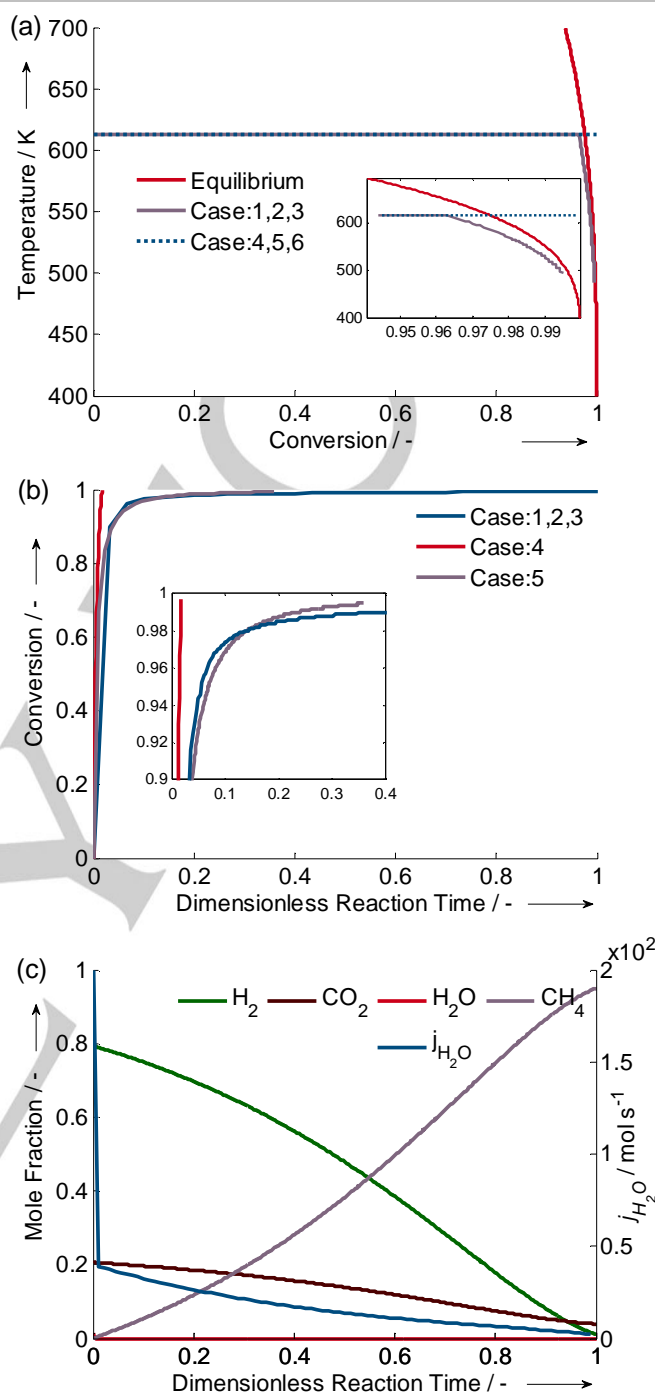


Figure 1. Results of Level 1, (a) Case 4,5,6 overcome the thermodynamic limitation: Equilibrium line is crossed, (b) Rate of conversion of case 1,4, and 5 (c) Optimal profile of T and H₂O extraction, (d) Mole fraction profile of Case 4 ($q(t)$, $j_{H_2O}(t)$)

steps are considered. The temperature inside the condenser is taken as decision variable in order to control the level of condensation. The second option is the continuous removal of H₂O by means of a membrane (membrane reactor). In this case, the water flux across the membrane is controlled by the membrane permeance.

The heat flux, q_{ex} , across the reactor is realized by an external coolant. The coolant temperature is a decision variable that varies to achieve an optimal temperature profile inside the reactor.

2.2.1 Reactor Cascade with Interstage Condensation

Condensation is a simple method for water removal. It is applicable here due to the high volatility of H₂, CH₄ and CO₂, which allows the removal of water without severe losses of H₂ and CH₄. The integration of condensation with the reaction in one unit allows the continuous extraction of water as found optimal in Level 1. However, since the methanation reactor operates at 613 K, the condensation is not feasible because it would require very high pressure (> 100 bar).

In our analysis in Level 2, we applied interstage condensation in a cascade of polytropic reactors where the number of condensation steps in the cascade is optimized. Since the objective is to maximize the STY, we selected randomly packed spherical catalytic particles that allow a maximum catalyst density. The particle diameter is a decision variable in the optimization and is constrained to: 1 mm ≤ D_p ≤ 30 mm. Other variables in the optimization for the reactors are: the inlet temperature (492 ≤ T_{in} ≤ 613 K), the inlet pressure (1 ≤ p_{in} ≤ 15 bar), the tube diameter (1 mm ≤ D_t ≤ 1 m), the number of tubes in the multitubular reactor (1 ≤ n_{tubes} ≤ 500), the inlet mole fraction, and the coolant temperature 422 ≤ T_c ≤ 613 K. For safety reasons, the temperature difference between the reaction mixture and the coolant is limited to be maximal 20 K.

2.2.1.1 Model Formulation of the Reactors

The reactors, operating in steady state, are modeled using a 1D pseudo-homogeneous plug flow model. According to Schelerth and Hinrichsen^[19], a 1D pseudo-homogeneous model is able to describe the qualitative trends of the reactor and can be used for evaluating the process conditions. The reactors are assumed to be radial gradient free in concentration, temperature or velocity and the axial diffusion is negligible compared to the axial convection.

The STY is defined as:

$$STY = \frac{\dot{n}_{CH_4, prod}}{t} \quad (4)$$

$$\frac{\rho}{4} D_t^2 \int_0^t \dot{\Omega}_{int} dt$$

The component mass balances (Eq. S6), the interstitial velocity profile (Eq. S7) and the superficial velocity (Eq. S8) are given in the Supplementary material.

The energy balance is modified according to the definition of Level 2 (see Eq. S9). The heat exchange, q_{ex} , between the reaction segment and the coolant section is limited in Level 2 (see Eqs. S10 to 12).

The pressure drop inside the reactor is estimated by the Ergun equation (see Eq. S13), and the bed porosity is described by the equation from Jeschar *et al.*^[20] (see Eq. S14).

To ensure a high effectiveness factor for the reaction rate ($h_c \geq 0.95$), criteria for the absence of inter and intra heat and mass transport limitations are enforced as constraints. For plug flow, the diameter ratio of the reactor tube to catalyst particle is constrained to be higher than ten. The equations are given in the Supplementary material (Eq. S15-S20).

2.2.1.2 Model Formulation for the Condensers

The phase separation in the condenser is calculated using an equilibrium flash model. At equilibrium, the dew point equation must be satisfied.^[21] The temperature and the split factor,

$x_i = \frac{n_{cond,ig}}{n_{cond,if}}$, are decision variables within the ranges:

$$0 \leq x_i \leq 1$$

$$298 \leq T_{cond} \leq 400 \text{ K.}$$

The pressure in the condenser, p_{conds} , is equal to the reactor outlet pressure preceding it. The solubility of the volatile components in liquid water is determined from the distribution

$$constants K_{cond,i} = \frac{y_{cond,i}}{x_{cond,i}} \quad [22]$$

The reactors, condensation steps, and the downstream drying step are all included in the optimization problem which has the following general form:

$$\max_{T_c(t), T_{cond}, \zeta_i, D_t, T_{in}, p_{in}, D_p} STY$$

s.t.

- Component mass balance (Eq. S6)
- Chemical reaction kinetics (Eqs. S1 to S4)
- Energy balance (Eq. S9)
- Ergun equation for pressure drop (Eq. S13)
- Transport kinetics (Eq. S10)
- State equations, e.g. ideal gas law
- Intrinsic bounds, e.g. temperature, tube diameters.
- Inlet and outlet compositions
- Design criteria equations (Eqs. S15 to S18)
- Dew point equation
- Mass balance for the glycol unit

2.2.1.3 Results and Discussion

The unlimited water removal as assumed in Level 1 could be realized by an infinite number of reactors integrated with an infinite number of condensation steps. However, this is not practical. In this study, reactor cascades with up to four condensation steps are considered.

Figure 5 shows the STY for the various cascades. As expected, the STY increases with increasing the number of condensation steps. In a cascade with four condensation steps (4CS), the calculated STY was 144 [molm⁻³s⁻¹] comparable to the value of 998 [molm⁻³s⁻¹] reached in Level 1.

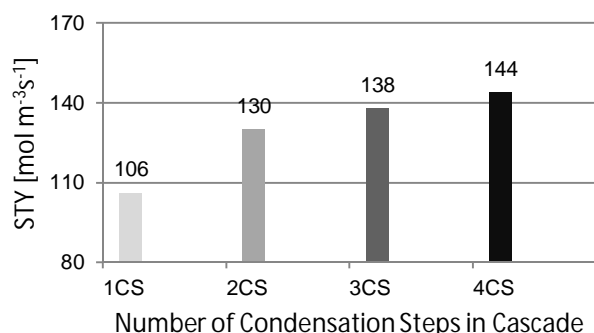


Figure 4 The STY of reactor cascades consisting of different number of condensation steps

By comparing the STYs in Fig. 4 one can notice that the incremental improvement in the STY decreases as a function of number of condensation steps. While a significant increase in the STY was calculated from 1CS (106 molm⁻³s⁻¹) to 2CS (130 molm⁻³s⁻¹) and 6.15% from 2CS to 3CS, an increase less than 5% is achieved between 3CS to 4CS. Based on the optimization results, one can conclude that a cascade with more than 2 condensation steps is likely economically unfeasible due to the minor improvement in the STY.

Table 2. Optimal operating conditions and inlet/outlet gas composition of Condenser 1 and 2

Condenser	1	2
T_{cond}	298	298
x [H ₂ , CO ₂ , CH ₄ , H ₂ O]	[1,1,1,0.008]	[1,1,1,0.01]
$x_{i,cond,in}$ [H ₂ , CO ₂ , CH ₄ , H ₂ O]	[0.43, 0.11, 0.15, 0.31]	[0.11, 0.04, 0.47, 0.38]
$x_{i,cond,out}$ [H ₂ , CO ₂ , CH ₄ , H ₂ O]	[0.62, 0.17, 0.21, 0.003]	[0.18, 0.07, 0.75, 0.006]

The 2CS cascade is thus the most attractive scheme and is therefore selected for a detailed analysis. Expectedly, the inlet pressure is at the upper bound (15 bar) since high pressure is favored for thermodynamic and kinetic reasons.

Figure 5 shows the mole fraction profiles of the components in the three reactors. The mole fraction of H₂O is relatively high in the Reactors 1 and 2 (R1 and R2) where most of the conversion is achieved ($X_{R1}=0.57$, $X_{R2}=0.94$).

The low split factor of water in condenser 1 and 2 (Table 3) following Reactor 1 and 2 respectively, implies that closely all water is in the liquid phase. As a result, the mole fraction of water decreases close to zero after each condensation step as can be seen at the inlet of Reactor 2 and 3.

On the other hand, the mole fraction of H₂O is relatively low in Reactor 3 that the thermodynamic limitation is overcome leading to a very high conversion ($X_{R4}=0.995$) at $T=575$ K. The gas mixture leaving Reactor 3 has a mole fraction of: 0.018 for H₂, 0.027 for CO₂, 0.862 for CH₄ and 0.093 for H₂O. H₂ and CO₂ concentrations already meet the pipeline specifications. CH₄ mismatches slightly the desired value while that of H₂O is far too

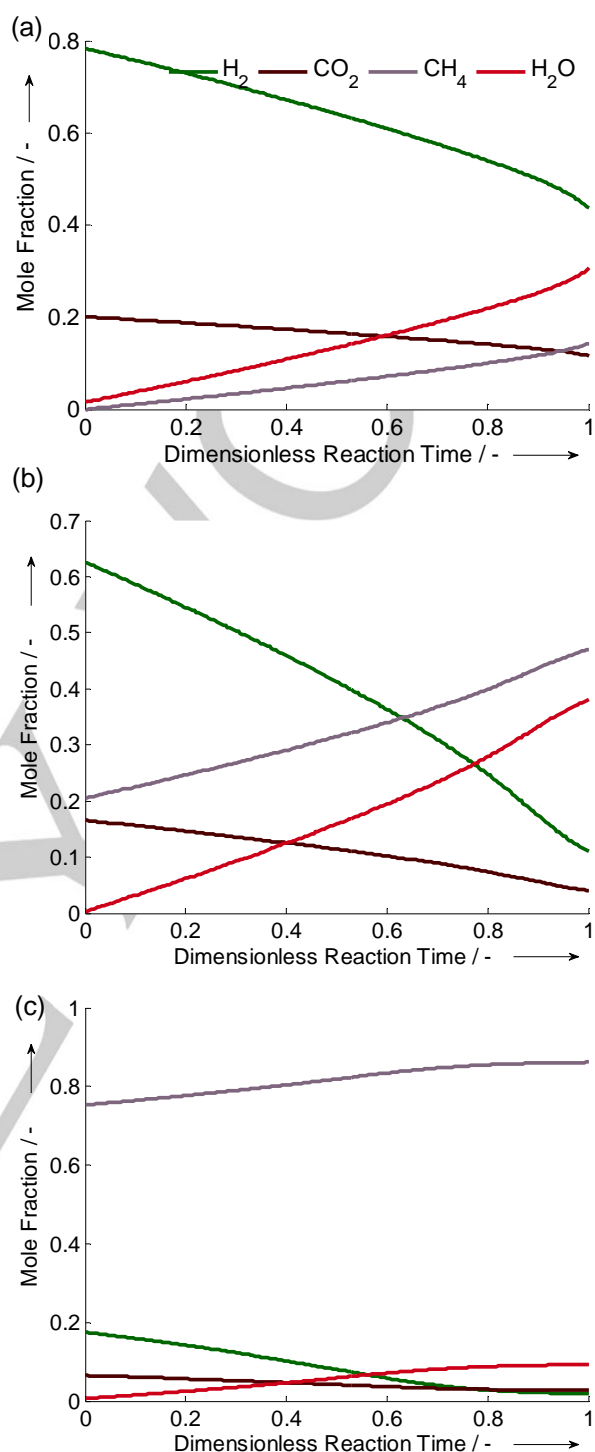


Figure 5. Results of 2CS cascade of Level 2, component mole fraction profile (a) in the 1st reactor, (b) in the 2nd reactor, (c) in the 3rd reactor

high. Nevertheless, the desired composition will be met after drying the gas.

Figure 6 shows the optimal temperature profile of the gas mixture and the coolant in the three reactors. At the beginning, the temperature increases gradually in parallel with the coolant temperature (see Fig. 6a). At the final stage, the coolant temperature increases very fast causing a steep increase in the

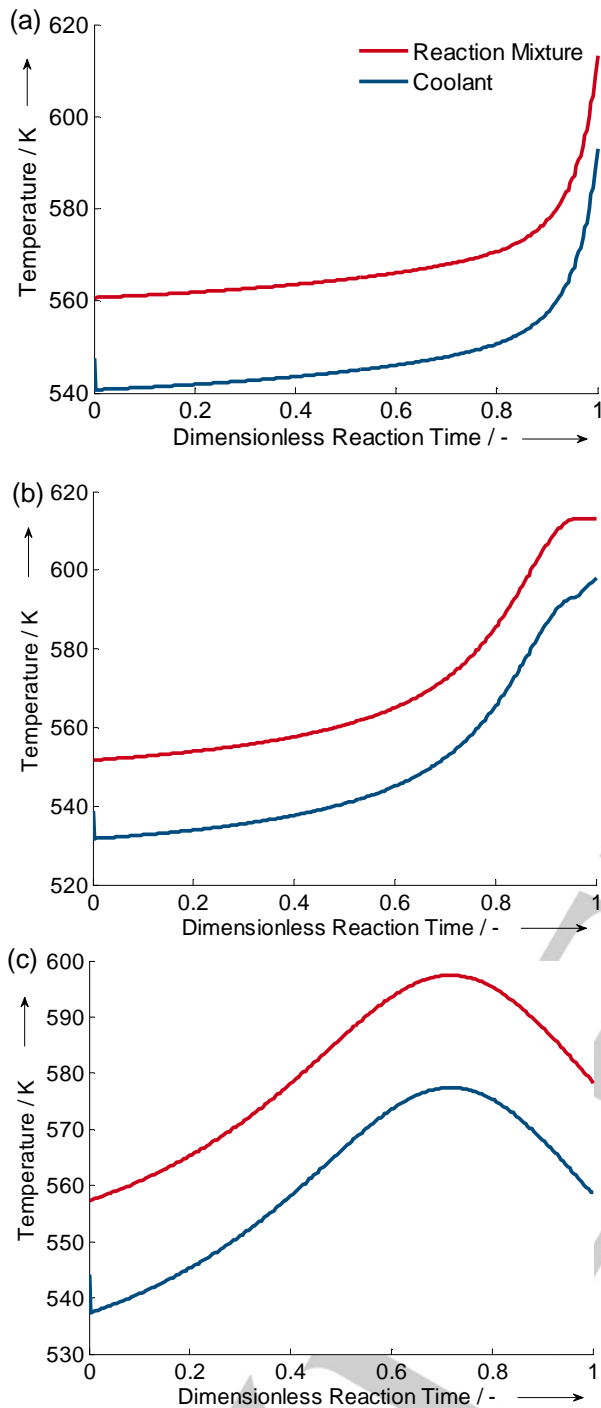


Figure 6. Results of 2CS cascade of Level 2, coolant and reaction mixture optimal temperature profile (a) in the 1st reactor, (b) in the 2nd reactor, (c) in the 3rd reactor

mixture temperature. The upper bound of the temperature is reached (613 K). The temperature difference between the coolant and the gas mixture remains 20 K allowing maximum possible heat transfer. The temperature profile is different than in Level 1 where the optimal temperature was constantly 613 K. The reason for the different optimal profiles is that in Level 1 the heat flux was assumed to be unlimited, i.e. any amount of heat released could be transferred instantaneously. The heat flux of Level 2 is limited by the heat transport kinetics as addressed earlier.

A similar behavior is seen in Reactor 2. At the beginning, the temperature increases gradually in parallel with the coolant temperature. At the final stage, the coolant temperature increases very fast causing a steep increase in the mixture temperature. In Reactor 3, the temperature increases faster at the beginning in comparison to Reactor 1 and 2 reaching a maximum (597 K). The coolant temperature then decreases gradually leading to a lower reaction temperature to achieve the desired conversion.

From the temperature profile of the coolant (increasing with time except for the last part of Reactor 3), one can deduce that the reactors should be coupled with co-current cooling.

2.2. Membrane Reactor

One process intensification concept is the application of a membrane reactor where the reaction and separation are integrated in one unit. Hydrophilic membranes are available for in-situ removal of water.^[23] However, for the present application, the membrane has to fulfill special requirements in terms of permeance, permselectivity, as well as thermal and mechanical stability. The hydroxy sodalite (H-SOD) membrane synthesized by Khajavi *et al.*^[24] possesses high H₂O/H₂ permselectivity allowing small molecules such as helium and water (kinetic diameters 2.6 and 2.65 Å respectively) to permeate through but not hydrogen. Exceptional for the H-SOD membrane is the high temperature (max. 723 K) and pressure (max 24 bar) tolerance.^[25]

2.2.2.1 Model for Membrane Packed Bed Reactor

The water flux through the membrane is described by a phenomenological transport kinetic model. The flux is proportional to the partial pressure difference across the membrane and the permeance:

$$j_{H_2O} = Perm(p_{H_2O} - p_{H_2O,s}) \cdot 10^5 \quad (5)$$

The permeance controls the flux and is allowed to vary within realistic bounds: $10^{-8} \leq Perm \leq 10^{-6} \text{ molm}^{-2}\text{Pa}^{-1}\text{s}^{-1}$. The equations for the mass and energy balances, the mass flux through the membrane, the interstitial velocity profile and the void fraction are presented in the Supplementary information.

The STY is defined based on the total volume of the membrane reactor as follows:

$$STY = \frac{\dot{n}_{CH_4, prod}}{t} \quad (6)$$

$$\frac{\rho}{4} D_{to}^2 \int_0^1 \dot{Q}_{int} dt$$

The general form of the optimization problem on Level 2 is given as follows:

$$\max_{T_c(t), Perm(t), D_{to}, D_{fi}, T_{in}, p_{in}, D_p}$$

s.t:

- Total mass balance (Eq. S6)
- Component mass balance (Eq. S6)

- Chemical reaction kinetics (Eqs. S1 to S4)
- Energy balance (Eq. S9)
- Ergun equation for pressure drop (Eq. S13)
- Transport kinetics (Eqs.5 and S10)
- State equations, e.g. ideal gas law
- Intrinsic bounds, e.g. temperature, tube diameters.
- Inlet and outlet compositions
- Mass balance for the glycol unit

2.2.2.2 Results and Discussion

Figure 7a shows the optimal H₂O flux profile along the reactor including the new control variable, the membrane permeance. The maximal permeance is applied (the upper bound $10^{-6} \text{ mol m}^{-2} \text{ s}^{-1} \text{ Pa}^{-1}$) over the entire reaction time. The water flux increases with the increase in water content (see Fig. 7a and 7b) reaching a maximum at the middle of the reactor.

An optimized inlet temperature of 532 K is obtained which then gradually increases in parallel with the coolant temperature. The temperature profile shows a steep increase at one third of the reaction time reaching the maximal allowed value (613 K). At this point, most of the reactants are already converted (see Fig. 7b). Then the temperature decreases again until the desired conversion is reached. The cooling duty is minimal since the temperature difference is small (4 K). The above described temperature profile could technically be realized by two reactor segments: First with active co-current and the second with counter current cooling.

A STY of $30 \text{ mol m}^{-3} \text{ s}^{-1}$ is obtained with the membrane reactor configuration, which is clearly lower than that of Case 4 in Level 1. The lower STY in a membrane reactor is partially attributed to the definition of STY. Here, the catalyst-free volume in the permeate side is included in the reactor volume unlike in Level 1 where the volume of the fluid element is assumed to be completely catalyst-filled. If the STY of a membrane reactor was defined based only on the catalyst-filled volume, then we obtain a STY of $35 \text{ mol m}^{-3} \text{ s}^{-1}$. Another reason is the limited heat and the water fluxes in the membrane reactor. Due to the limited permeance of the membrane (Eq. 5) this reactor had higher water mole fraction than those demonstrated in Level 1 (Fig. 3) or Level 2 for the reaction cascade (Fig. 5).

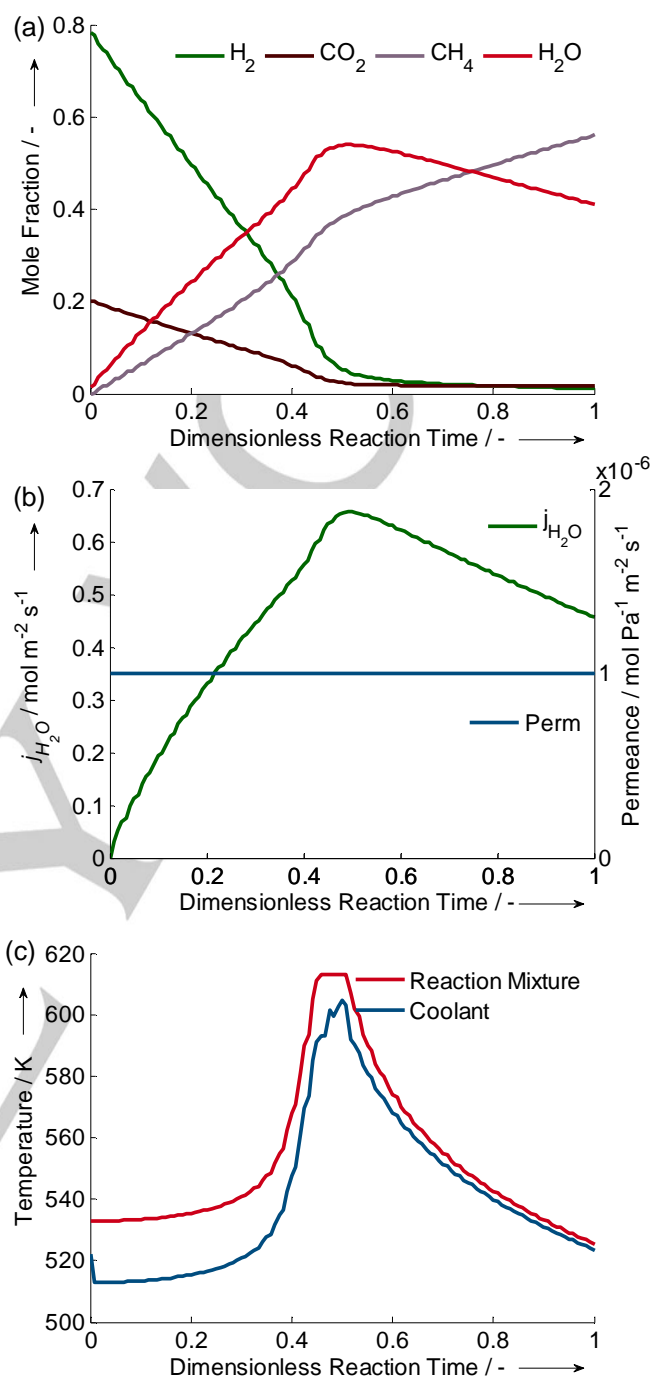


Figure 7. Results of membrane reactor, (a) Permeance and water flux optimal profiles, (b) Component mole fraction profile, (c) Optimal temperature profile of the coolant and the reaction mixture

2.3 Comparison between Reactor Cascade and Membrane Reactor:

By comparing the STY of the membrane reactor ($\text{STY}=30 \text{ mol m}^{-3} \text{ s}^{-1}$) to the reactor cascades with interstage condensation ($\text{STY}=130 \text{ mol m}^{-3} \text{ s}^{-1}$), one can see that the 2CS cascade is the most attractive configuration. It offers a STY that is more than 300% larger than the membrane reactor.

Improvements in the membrane permeance are crucial for enhancing the reactor performance. Increasing the permeance

by one order of magnitude (to $10^{-5} \text{ molPa}^{-1}\text{m}^{-2}\text{s}^{-1}$) would increase the STY by more than 130% ($\text{STY}=70 \text{ molm}^{-3}\text{s}^{-1}$).

2.3 Level 3

The technical feasibility of the most promising reaction configuration, 2CS reactor cascade, is further assessed in the following. The same equations and bounds as used in the previous level are applied in Level 3. However, the balance equations are now formulated in the Eulerian formulation (see Eqs. S26 to S28). The optimal temperature profiles of the three reactors in Level 2 are technically approximated using co-current cooling. The coolant used is molten salt NaNO_2 (HITECH[®] from BRENNTAG) which is suitable for high temperature applications (422-811 K).

The change in the coolant temperature is now defined by a simplified 1D energy balance. The mass flow rate of the coolant, \dot{n}_c , is a decision variable (see Eq. S29).

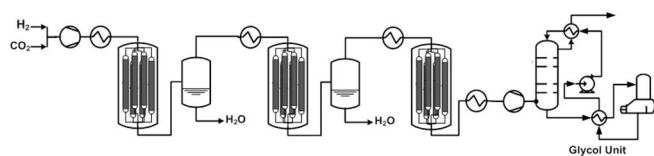


Figure 8 Schematic representation of the 2CS cascade integrated with the downstream drying step

The energy balance for the cooling section reduces the degrees of freedom of the optimization problem. The heat flux can not be optimized anymore and only the inlet conditions (e.g. T_{in} , p_{in}) and other design variables (e.g. D_t , D_p) are optimized. This will result in a lower STY in Level 3 compared to that in Level 2.

2.3.1 Results and Discussion

Figure S1 shows the temperature profiles of the gas mixture and the coolant in the three reactors. The mixture temperature profiles in Level 3 resembled the profiles of Level 2 except for the steep increase seen at the end of Reactor 1 and 2 in Level 2. The maximum temperature reached was around 562 K in Reactors 1 and 2 and 580 K in Reactor 3.

Although the STY achieved in Level 3 ($94 \text{ molm}^{-3}\text{s}^{-1}$) is smaller than the one achieved in Level 2 ($130 \text{ molm}^{-3}\text{s}^{-1}$), the result shows good temperature control with relatively small reactor sizes.

The constructional parameters of the reactor tubes in the three reactors are listed in Table 4. The optimized length of the tubes is much larger than their respective diameter which was at its lower bound. This is related to the high exothermicity of the reaction which demands a geometry that provides a large surface area to volume ratio for an efficient heat transfer between the gas mixture and the coolant.

The particle diameter is at its lower bound (1 mm) in the three reactors. The smaller the particle diameter, the less limited is the heat and mass transfer. Moreover, a small particle diameter lowers bed porosity and increases the catalyst density. The optimal ratio of H_2 to CO_2 in the feed is 3.9 and the optimal number of tubes in the reactor is 218.

Table 3. The geometric design and operation conditions of the different reactors in the 2CS cascade.

Reactor	1	2	3
D_t [cm]	1	1	1
D_p [mm]	1	1	1
L [m]	1	0.94	0.37
T_{in} [K]	553	544	547
T_{out} [K]	560	561	574
$x_{i,in}$ [$\text{H}_2, \text{CO}_2, \text{CH}_4, \text{H}_2\text{O}$]	[0.78 0.2 0.0 0.015]	[0.6 0.16 0.24 0.003]	[0.23 0.077 0.69 0.006]
$x_{i,out}$ [$\text{H}_2, \text{CO}_2, \text{CH}_4, \text{H}_2\text{O}$]	[0.4 0.11 0.16 0.34]	[0.16 0.05 0.47 0.32]	[0.02 0.03 0.83 0.13]
X_{out}	0.62	0.92	0.995
$\dot{n}_{i,in}$ [mols^{-1}]	0.093	0.047	0.024

Conclusion

A reaction configuration was optimized to produce renewable methane of natural gas grid quality while reducing the downstream processing steps to dehydration. The influence of ideal cooling/heating and dosing/removal of the different components on maximizing the STY was systematically investigated according to the EPF principles. Extraction of water is clearly more beneficial than the removal of CH_4 leading to a significantly increased STY. Therefore, two reaction configurations that apply water removal were investigated and compared: Membrane reactor with continuous water removal over the entire reaction time and polytropic reactor cascade with intermediate condensation. In this work, the cascade was optimized in terms of the temperature profile of the reaction mixture, operating pressure, inlet composition, reactor dimensions, number of condensation steps, the moment along the reaction time at which condensation needs to be performed and the level of separation (split factor).

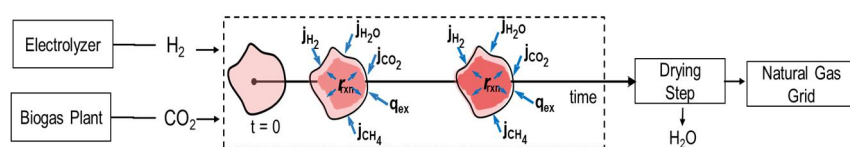
Our theoretical analysis shows that a cascade consisting of three multitubular reactors with co-current cooling and two condensation steps was the most attractive configuration in terms of maximized STY. The reactor cascade approach is superior to the membrane reactor. Nevertheless, the membrane reactor is still an attractive option for the Sabatier process and shouldn't be completely ruled out. The performance of the membrane reactor could be significantly enhanced by improving the permeance of the membrane material. The calculations showed that an increase in the membrane permeance by one order of magnitude from the typical value ($10^{-6} \text{ molPa}^{-1}\text{m}^{-2}\text{s}^{-1}$)

increases the STY by 130%. Moreover, the membrane reactor is more compact than the cascade configuration where additional auxiliary units are needed giving rise in the investment and operating costs. In order to identify the economically best reaction configuration a detailed optimization based on cost estimation would be necessary.

Keywords: CO₂ methanation • Dynamic optimization • Energy conversion • Reactor design • Renewable resources

- [1] S. Schieban, Grube, T., Robinius, M., Zhao, L., Otto, A., Kumar, B., Weber M., Stolten, D., in *Transition to Renewable Energy Systems*, **2010**, pp. 813-848.
- [2] (a) J. Kopyscinski, T. J. Schildhauer, S. M. A. Biollaz, *Fuel* **2010**, *89*, 1763-1783; b) M. Sudiro, A. Bertucco, *Natural Gas* **2010**, 105-126.
- [3] M. A. A. Aziz, A. A. Jalil, S. Triwahyono, A. Ahmad, *Green Chemistry* **2015**, *17*, 2647-2663.
- [4] (a) W. Wang, J. Gong, *Frontiers of Chemical Engineering in China* **2011**, *5*, 2-10; (b) J. J. Gao, Q. Liu, F. N. Gu, B. Liu, Z. Y. Zhong, F. B. Su, *Rsc Advances* **2015**, *5*, 22759-22776.
- [5] M. Appl, in *Ullmann's Encyclopedia of Industrial Chemistry*, **2011**.
- [6] (a) M. De Saint Jean, P. Baurens, C. Bouallou, K. Couturier, *International Journal of Hydrogen Energy* **2015**, *40*, 6487-6500; (b) M. De St Jean, P. Baurens, C. Bouallou, *International Journal of Hydrogen Energy* **2014**, *39*, 17024-17039.
- [7] T. Schaaf, J. Grünig, M. R. Schuster, T. Rothenfluh, A. Orth, *Energy, Sustainability and Society* **2014**, *4*, 1-14.
- [8] A. El Sibai, L. Rihko-Struckmann, K. Sundmacher, in *12th International Symposium on Process Systems Engineering and 25th European Symposium on Computer Aided Process Engineering, Vol. 37* (Eds.: K. V. Gernaey, J. K. Huusom, R. Gani), **2015**, pp. 1157-1162.
- [9] L. Kiewidt, J. Thoming, *Chemical Engineering Science* **2015**, *132*, 59-71.
- [10] M. Götz, A. M. Koch, F. Graf, in *International Gas Union Research Conference Proceedings (IGRC), Vol. 1*, January ed., **2014**, pp. 314-327.
- [11] M. Götz, J. Lefebvre, D. Schollenberger, S. Bajohr, R. Reimert, T. Kolb, in *International Gas Union Research Conference Proceedings (IGRC), Vol. 3*, January ed., **2014**, pp. 2313-2320.
- [12] H. Ohya, J. Fun, H. Kawamura, K. Itoh, H. Ohashi, M. Aihara, S. Tanisho, Y. Negishi, *Journal of Membrane Science* **1997**, *131*, 237-247.
- [13] J. D. Holladay, K. P. Brooks, R. Wegeng, J. Hu, J. Sanders, S. Baird, *Catalysis Today* **2007**, *120*, 35-44.
- [14] K. P. Brooks, J. L. Hu, H. Y. Zhu, R. J. Kee, *Chemical Engineering Science* **2007**, *62*, 1161-1170.
- [15] H. Freund, K. Sundmacher, *Chemical Engineering and Processing* **2008**, *47*, 2051-2060.
- [16] F. Koschany, D. Schlereth, O. Hinrichsen, *Applied Catalysis B: Environmental* **2016**, *181*, 504-516.
- [17] (a) A. Peschel, H. Freund, K. Sundmacher, *Industrial & Engineering Chemistry Research* **2010**, *49*, 10535-10548; (b) A. Peschel, F. Karst, H. Freund, K. Sundmacher, *Chemical Engineering Science* **2011**, *66*, 6453-6469; (c) B. Hentschel, A. Peschel, H. Freund, K. Sundmacher, *Chemical Engineering Science* **2014**, *115*, 69-87.
- [18] N. A. Zhilyaeva, E. A. Volnina, M. A. Kukina, V. M. Frolov, *Petroleum Chemistry* **2002**, *42*, 367-386.
- [19] D. Schlereth, O. Hinrichsen, *Chemical Engineering Research & Design* **2014**, *92*, 702-712.
- [20] J. Jeschar, *Archiv für das Eisenhüttenwesen* **1964**, *35*, 91-108.
- [21] L. T. Biegler, I. E. Grossmann, A. W. Westerberg, *Systematic methods of chemical process design*, Prentice Hall, Upper Saddle River, NJ, **1997**.
- [22] R. Fernandez-Prini, J. L. Alvarez, A. H. Harvey, *Journal of Physical and Chemical Reference Data* **2003**, *32*, 903-916.
- [23] J. Corona, J. Santamaria, *Separation and Purification methods* **1999**, *28*, 127-177.
- [24] S. Khajavi, F. Kapteijn, J. C. Jansen, *Journal of Membrane Science* **2007**, *299*, 63-72.
- [25] (a) S. Khajavi, S. Sartipi, J. Gascon, J. C. Jansen, F. Kapteijn, *Microporous and Mesoporous Materials* **2010**, *132*, 510-517; (b) S. Khajavi, J. C. Jansen, F. Kapteijn, *Journal of Membrane Science* **2009**, *326*, 153-160.

Table of Contents



Optimal design of Sabatier reactor for power to gas applications . CO₂ methanation reactor was systematically analyzed and optimized using the flux oriented Elementary Process Function methodology. The potential of different enhancement concepts: cooling/heating and dosing/removal of different components is investigated. The best concept for maximizing space time yield is technically realized.